Formation of gold clusters on TiO_2 from adsorbed $Au(CH_3)_2(C_5H_7O_2)$: characterization by X-ray absorption spectroscopy

Javier Guzman, Stefan Kuba, Juan C. Fierro-Gonzalez, and Bruce C. Gates*

Department of Chemical Engineering and Materials Science, University of California, Davis, California 95616, USA

Received 2 October 2003; accepted 14 March 2004

Gold nanoclusters on TiO_2 powder were prepared from adsorbed $Au^{III}(CH_3)_2$ ($C_5H_7O_2$) (dimethyl acetylacetonate gold(III)) and characterized by extended X-ray absorption fine structure (EXAFS) and X-ray absorption near edge structure (XANES) spectroscopies. The samples were tested as catalysts for CO oxidation at 298 K and atmospheric pressure and characterized by EXAFS and XANES with the catalysts in the working state. The XANES results identify Au(III) in the initially prepared sample, and the EXAFS data indicate mononuclear gold complexes as the predominant surface gold species in this sample, consistent with the lack of Au–Au contributions in the EXAFS spectrum. The mononuclear gold complex is bonded to two oxygen atoms of the TiO_2 surface at an Au–O distance of 2.16 Å. Treatment of this complex in He or in H_2 at increasing temperatures led to formation of metallic gold clusters of increasing size, ultimately those with an average diameter of about 15 Å. The data demonstrate the presence of metallic gold clusters in the working catalysts and also show these clusters alone are not responsible for the catalytic activity.

KEY WORDS: CO oxidation; EXAFS; gold; gold clusters; TiO_2; XANES; X-ray absorption spectroscopy.

1. Introduction

Highly dispersed gold nanoclusters supported on metal oxides have been inferred to be active catalysts for reactions including oxidation of CO [l–3], selective oxidation of propene [4,5], reduction of NO [6], and hydrochlorination of acetylene [7]. The properties of these catalysts depend on the support [8], synthesis method [9,10], and pretreatment conditions [11,12]. TiO_2 supports provide some of the most active gold catalysts. TiO_2-supported catalysts prepared from precursors such as $HAuCl_4$ [9] and $Au(PPh_3)(NO_3)$ [10] typically contain components such as chlorine or phosphorus, which affect the catalytic properties. The nature of the active sites and the sizes and structures of the gold nanoclusters in these catalysts remain to be determined.

Our goal was to prepare and characterize TiO_2-supported nanoclusters of gold under conditions to make them extremely small, highly dispersed, and free of complicating components such as chlorine and phosphorus. We attempted to correlate the cluster size and oxidation state(s) of gold with catalytic activity for CO oxidation. We report the synthesis of TiO_2-supported gold nanoclusters from $Au^{III}(CH_3)_2(acac)$ (acac is $C_5H_7O_2$) [13], their characterization by extended X-ray absorption fine structure (EXAFS) spectroscopy and X-ray absorption near edge structure (XANES), and data representing their catalytic activity for CO oxidation. $Au^{III}(CH_3)_2(acac)$ was chosen as the precursor because it has organic ligands that are readily removed under mild treatment conditions.

Our strategy involved a variation of the cluster size and oxidation state of gold by controlling the aggregation to form highly dispersed gold clusters by choice of the treatment temperature and atmosphere. The data give evidence of (a) the formation of mononuclear Au(III) complexes as the predominant initial surface gold precursors; (b) their conversion into supported clusters with an average diameter of about 15 Å by treatment in He or H_2; and (c) the presence of metallic gold in the working catalysts along with evidence that the catalytic sites are more complicated than just gold clusters.

2. Experimental

2.1. Materials

H_2 was supplied by Matheson (99.999%) or generated by electrolysis of water in a Balston generator (99.99%) and purified by passage through traps containing reduced Cu/Al_2O_3 and activated zeolite 4A to remove traces of O_2 and moisture, respectively. He (Matheson, 99.999%) was purified by passage through similar traps. O_2 (Matheson, 99.999%) in a 20% mixture in He was used as received. CO (Matheson, 99.999%) in a 10% mixture in He was purified by passage through a trap containing activated γ-Al_2O_3 particles and zeolite 4A to remove any traces of metal carbonyls from the high-pressure gas cylinder and moisture, respectively. The TiO_2 support (Degussa,

*To whom correspondence should be addressed.
E-mail: bcgates@ucdavis.edu

1011-372X/04/0500–0077/0 © 2004 Plenum Publishing Corporation

P25 TiO_2; approximately 30% rutile and 70% anatase) was calcined in O_2 at 673 K for 2 h, immediately followed by evacuation of the sample for 14 h at 673 K. The TiO_2 was then cooled to room temperature under vacuum, isolated, and stored in a N_2-filled drybox until it was used. *n*-Pentane solvent (Fisher, 99%) was dried and purified by refluxing over sodium/benzophenone ketyl and deoxygenated by sparging of N_2. The precursor $Au(CH_3)_2(acac)$ [dimethyl(acetylacetonate) gold(III)] (Strem, 98%) was used as supplied.

2.2. Sample synthesis

The syntheses and transfers of samples were performed with exclusion of air and moisture on a double-manifold Schlenk vacuum line and in a glove box purged with N_2 that was recirculated through traps containing particles of supported Cu and zeolite 4A for removal of O_2 and moisture, respectively. The sample, containing 1 wt% Au, was prepared by slurrying $Au(CH_3)_2(acac)$ in *n*-pentane with TiO_2 powder that had been partially dehydroxylated under vacuum at 673 K. The slurry was stirred for 1 day and the solvent removed by evacuation (pressure $< 10^{-3}$ Torr) for 1 day. The resultant TiO_2-supported gold sample was treated in flowing He or H_2 at atmospheric pressure as the temperature was ramped at a rate of 3 K min^{-1} from room temperature to a temperature in the range of 323–373 K.

2.3. X-ray absorption spectroscopy (XAS)

The XAS experiments were performed at beamline X-11A at the National Synchrotron Light Source (NSLS), Brookhaven National Laboratory, Upton, NY. The storage ring electron energy was 2.5 GeV, and the ring current varied within the range of 110–250 mA. Spectra were collected in the fluorescence mode, which was chosen rather than the transmission mode because of the high absorbance by Ti at the Au L_{III} edge (11919 eV). Higher harmonics in the X-ray beam were minimized by detuning the Si(lll) double crystal monochromator by 20–25% at the Au L_{III} edge (11919 eV). The Ge detector with 13 channels allowed recording of 13 signals per scan, and each reported spectrum is the average of seven scans.

Data were recorded during CO oxidation catalysis at 373 K and also with the catalysts in flowing He and in H_2 at atmospheric pressure and at a temperature in the range of 323–573 K. In an argon-filled drybox at the synchrotron, 0.3 g of powder sample was loaded into a XAS cell/reactor (the powder catalyst was held in the middle of a XAS cell/reactor by glass wool plugs), which was then isolated, removed from the glove box, and installed in the flow system at the beamline without contacting of the catalyst with air or moisture. The XAS cell/reactor is well approximated as a plug-flow reactor.

2.4. CO oxidation catalysis

CO oxidation catalysis was carried out at atmospheric pressure and 298 K in a standard once-through, nearly isothermal tubular packed-bed flow reactor. The catalyst (0.05 g, mixed in a mass ratio of 1:50 with particles of inert, nonporousα-Al_2O_3) was loaded into the reactor in a glove box and transferred to a flow system without contacting air. Total feed flow rate to the reactor was l00 mL (NTP) min^{-1} with a CO partial pressure of 11 Torr and an O_2 partial pressure of 11 Torr (and the remainder He). The conversions were determined by gas chromatographic analysis of the product stream; the conversions were determined on the basis of CO and O_2 consumption and CO_2 formation with an accuracy of about $\pm 5\%$. The conversion is defined as the number of moles of CO that reacted to produce CO_2, divided by the initial number of moles of CO in the feed. An on-line gas chromatograph (Hewlett-Packard, HP-589 Series II) equipped for column switching in combination with two-channel detection (with a thermal conductivity detector and a flame-ionization detector) [14], was used to separate any water that might have been present from other product gases in a polar column (Hayesep Q, 8′ × 1-8″, 80–100 mesh), followed by separation of O_2, CO, and CO_2 in a zeolite 5A column (Chrompack, PLOT Fused Silica, 25-m × 0.53-mm).

3. Analysis of EXAFS data

Analysis of the EXAFS data was carried out with a difference file technique [15–17] by use of the software XDAP [18]. No attempt was made to account for the small atomic X-ray absorption fine structure (AXAFS) [19,20] (the low-*r* portion; *r* is the distance from the absorber atom, Au) of the spectrum other than by application of standard background subtraction techniques [21]. Iterative fitting was carried out until excellent agreement was attained between the calculated k^0-, k^1-, and k^2-weighted data (*k* is the photoelectron wave vector) and the postulated model [15–17].

Experimentally determined reference files prepared from EXAFS data representing materials of known structure were used in the analysis. EXAFS data characterizing a gold foil and $Na_2Pt(OH)_6$ were used for the phase shifts and backscattering amplitudes of the Au–Au and Au–$O_{support}$ interactions. (The transferability of the phase shifts and backscattering amplitudes for neighboring atoms in the periodic table has been justified experimentally [22]). $Au(CH_3)_2(acac)$ mixed with SiO_2 was used to obtain the phase shifts and backscattering amplitudes for analysis of the Au–C and Au–O interactions.The Au–Ti reference file was calculated by using the codes FEFF 7.0 and FEFF 8.0 [23] and structural parameters representing $AuTi_3$ [24].

Details of the preparation of the reference files are presented elsewhere [25,26].

The number of parameters used in fitting the data to each model is justified statistically by the Nyquist theorem [27]. The fitting ranges in both momentum space and real space were determined by the data quality. The quality of the fitting was confirmed by the values of fit diagnostic parameters, ε_v^2 (goodness of fit) [27] and the variances between the data and model predictions for the EXAFS function χ and the Fourier transform of χ (for k^0-, k^1-, and k^2-weighting of the data). No corrections for self-absorption were included in the analysis.

The X-ray absorption edge energy was calibrated with the measured signal of a gold foil (at the Au L_{III} edge, 11919 eV) scanned simultaneously with the sample. The edge is represented as the inflection point at the first absorption peak, at nearly 119191 eV. The data were normalized by dividing the absorption intensity by the height of the absorption edge.

4. Results

4.1. Spectroscopic evidence of oxidation states of gold

XANES provides information about the oxidation states and site symmetries of the gold. XANES peak locations and intensities characterizing reference materials containing gold in various oxidation states, summarized elsewhere [28–30], provide a basis for interpretation of the data. The XANES characterizing complexes containing Au(III) show a prominent feature (white line) in the Au L_{III} near-edge region, centered at an energy 4 eV higher than that of the Au L_{III} X-ray absorption edge. This absorption peak is missing from the spectra of metallic gold because of the complete occupancy of the *d* states (the gold ground state electron configuration is $[Xe]4f^{14}5d^{10}6s^1$). Furthermore, the spectrum of Au(III) shows a shoulder at an energy 15 eV and a broad shoulder at 50 eV higher than that of the X-ray absorption edge, whereas the spectrum of Au(0) shows a shoulder at 15 eV and intense peaks at 25 and 50 eV higher than that of the Au L_{III} edge [28–30].

XANES of our initially prepared TiO_2-supported sample clearly indicates the presence of Au(III), identified by the intense peak at 4 eV, a shoulder at 15 eV, and a broad shoulder at 50 eV above the X-ray absorption edge (figure 1). The decrease in the area under the white line with increasing temperature of treatment in He (figure 1a) or H_2 (figure 1b) indicates increasing reduction of the gold by conversion of cationic gold into gold in a lower oxidation state; ultimately the gold had metallic character, as evident from the absence of a peak at 4 eV and the presence of a shoulder at 15 eV and intense peaks at 25 and 50 eV higher than the energy of the Au L_{III} edge.

4.2. Formation of gold clusters from supported gold complexes

EXAFS spectroscopy was used to characterize the structures of the gold complexes formed by adsorption of $Au(CH_3)_2(acac)$ on TiO_2 and the gold clusters formed from the complexes by treatment in flowing He or H_2 at various temperatures. Analysis of the EXAFS data (figure 2) gave the parameters shown in table 1 representing the initially prepared sample; these indicate site-isolated mononuclear gold complexes. The lack of Au–Au first- and second-shell contributions ($N_{Au-Au} = 0.0$) indicates the site isolation of the complexes and lack of detectable gold clusters in the sample [31]. The Au–O coordination number of 2.0 and a distance of 2.16 Å show that each Au atom was bonded to two oxygen atoms, inferred to be part of the TiO_2 surface; the Au–O distance is typical of metal-oxygen bonding distances in other oxide- and zeolite-supported mononuclear complexes of group 8 metals [31,32].

Consistent with our results, metal complexes incorporating nucleophilic ligands such as acac have been shown to react with OH groups of oxide surfaces [33], typically by ligand exchange, resulting in the displacement of a ligand from the metal center of the complex to the support surface and the concomitant formation of bonds between the metal and support oxygen or OH groups.

EXAFS data characterizing the sample that was treated in He or H_2 at increasing temperatures ranging from 373 to 573 K (figure 3) were analyzed to give the parameters shown in table 2. The data show that as the treatment temperature increased, the Au–Au first-shell coordination number increased, as increasingly large gold clusters formed. The first-shell Au–Au coordination numbers increased monotonically, being 5.1 after exposure of the sample to He at the lowest treatment temperature (373 K) and 7.1 after exposure of the sample to He at the highest treatment temperature (573 K), corresponding to an increase in the average cluster diameter from about 9 Å to about 15 Å, as determined from models [34] that relate the average cluster size to the EXAFS first-shell metal–metal coordination number. Thus, we infer that the supported gold species migrated readily on the TiO_2 surface as reduction and aggregation occurred.

Besides the changes in nuclearity and size of the TiO_2-supported gold clusters during He and H_2 treatments, the structural parameters determined by EXAFS spectroscopy that characterize the metal cluster–support interaction were altered, as indicated by the changes in Au–O contributions (tables 1 and 2).

4.3. CO oxidation catalysis

The untreated sample consisting of mononuclear Au(III) complexes as well as the samples treated for 1 h in He at 373, 473, or 573 K to form gold clusters were

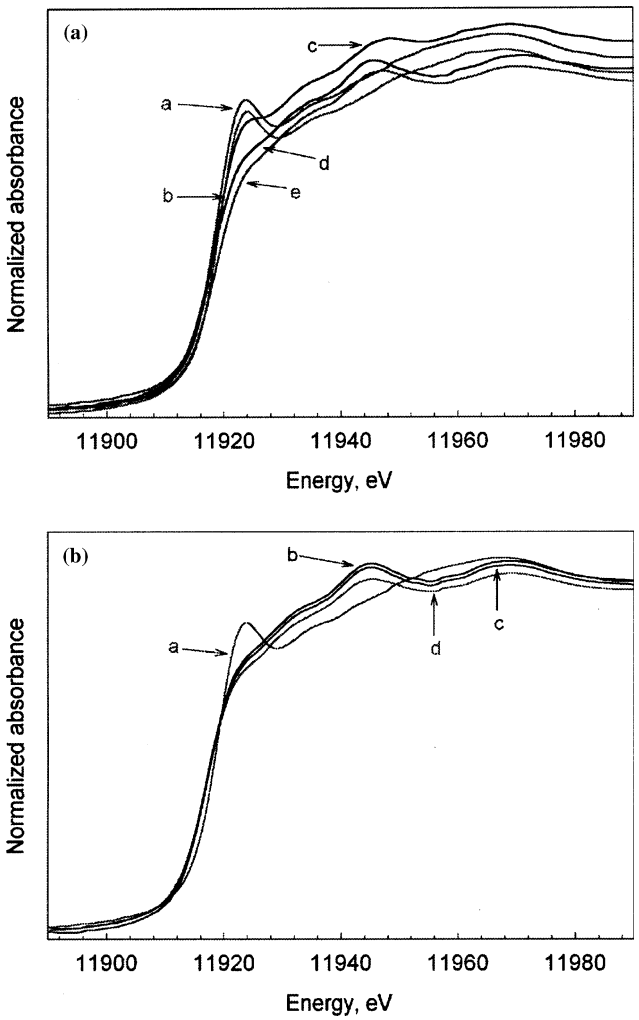

Figure 1. XANES data at the Au L_{III} edge characterizing TiO_2-supported gold samples. **(a)** Scanned after (a) adsorption of $Au(CH_3)_2(acac)$ and after subsequent exposure to He at the following temperatures (K): (b) 323, (c) 373, (d) 473, and (e) 573. **(b)** Scanned after (a) adsorption of $Au(CH_3)_2(acac)$ and after subsequent exposure to H_2 at the following temperatures (K): (b) 373, (c) 473, and (d) 573.

tested for room-temperature CO oxidation catalysis, with the partial pressures of the components in the reactant stream being $P_{CO} = 11$ Torr, $P_{O_2} = 11$ Torr, and $P_{He} = 738$ Torr. Each catalyst was active for CO oxidation, with conversions > 10% at low times on stream. In each case, the only product observed was CO_2, and there was no measurable conversion of CO and O_2 in the presence of TiO_2 alone. Except for the catalyst pretreated at 573 K in He, each catalyst deactivated completely or almost completely within 1 h of operation. In contrast, the catalyst pretreated at 573 K in He was not completely deactivated; the conversion was stable at about 10% after the initial deactivation (rate $\approx (4 \pm 0.2) \times 1.0^{-2}$ mol_{CO_2} $mol_{Au^{-1}}$ s^{-1} [Rate values were calculated on the basis of the assumption that each Au atom in the sample was available for catalysis; thus the values underestimate the real rate.]

The dependence of the CO conversion on time on stream characterizing the untreated catalyst as well as that characterizing the catalysts pretreated in He at temperatures ranging from 373 to 573 K is shown in figure 4. Except for the sample treated in He at 573 K (characterized by an initial conversion of about 50%), the observed conversion maxima at low TOS were about the same for each sample, in the range of 13% to 21% [the approximate rates are in the range of $(5–8 \pm 0.3) \times 10^{-2}$ mol_{CO_2} $mol_{Au^{-1}}s^{-1}$)]. The maximum rate characterizing the catalyst pretreated at 573 K in He is of the same order of magnitude as those reported for TiO_2-supported catalysts prepared from gold precursors different from ours [8].

4.4. *X-ray absorption spectra of functioning CO oxidation catalysts*

Expecting that the degree of oxidation and of aggregation of the gold might be dependent on the conditions of catalysis, we investigated the structure and oxidation state of the gold with EXAFS and XANES during CO oxidation catalysis.

The XANES characterizing the as-prepared sample, initially containing TiO_2-supported Au(III) complexes, during CO oxidation catalysis at 373 K and 760 Torr (11 Torr of O_2, 11 Torr of CO, and the balance He) show that the oxidation state of gold was reduced from +3 to 0 during catalysis in the flow system, as shown by the reduction and eventual disappearance of the intense peak at an energy 4 eV higher than that of the X-ray absorption edge and the appearance of the features characteristic of metallic gold (a shoulder at 15 eV and intense peaks at 25 and 50 eV higher than the Au L_{III} edge, figure 5). In contrast, the XANES characterizing the samples that had been treated in He or H_2 at 573 K, containing gold clusters (as shown above), during catalysis at 373 K and 760 Torr (11 Torr of O_2, 11 Torr of CO, and the balance He) did not show any evidence of changes during catalysis, retaining the characteristic features of metallic gold (figure 6).The EXAFS data characterizing the as-prepared sample during CO oxidation catalysis at 373 K and 760 Torr (11 Torr of O_2, 11 Torr of CO, and the balance He) show that over the period of an hour onstream, the gold complexes aggregated to form metallic gold clusters about 15 Å in average diameter, as calculated from the first- and second-shell Au–Au coordination numbers (table 3).

Similarly, the sample that had been treated in He at 575 K to form metallic gold clusters of about 15 Å in average diameter was characterized by EXAFS spectroscopy during catalysis. The data indicate retention of the initial average cluster size, as indicated by the lack of changes in the first- and second-shell Au–Au coordination numbers (table 4).

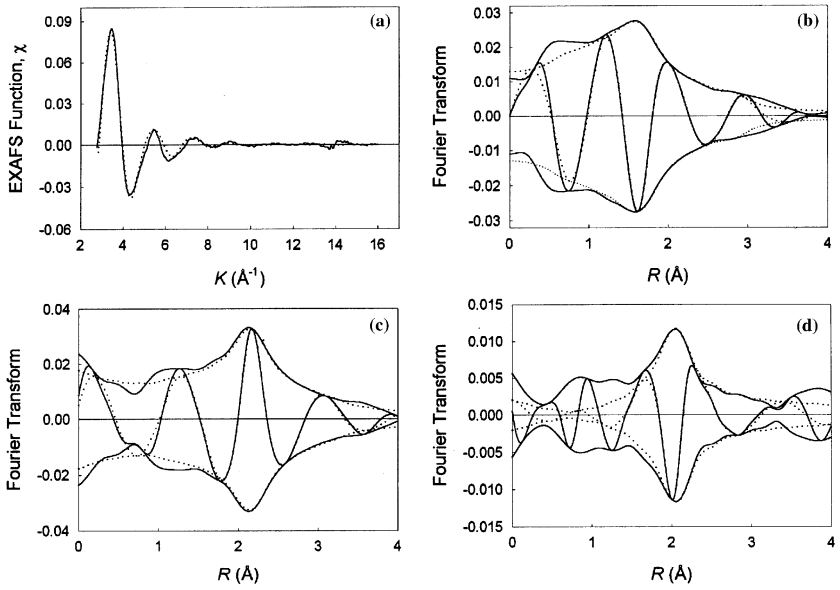

Figure 2. Results of EXAFS analysis characterizing the TiO_2-supported gold sample formed by adsorption of $Au(CH_3)_2(acac)$ at 1 atm and 298 K: (a) Experimental EXAFS function (solid line) and sum of the calculated Au–O_s + Au–O_l + Au–Ti contributions (dashed line). (b) Imaginary part and magnitude of uncorrected Fourier transform (k^0 weighted) of experimental EXAFS function (solid line) and sum of the calculated Au–O_s + Au–O_l + Au–Ti contributions (dashed line). (c) Residual spectrum illustrating the Au–O_s contribution; imaginary part and magnitude of phase- and amplitude-corrected Fourier transform (k^0 weighted) of experimental data minus the calculated Au-O_l + Au–Ti contributions (solid line) and calculated Au–O_s contribution (dashed line). (d) Residual spectrum illustrating the Au–O_l contribution; imaginary part and magnitude of phase- and amplitude-corrected Fourier transform (k^0 weighted) of experimental data minus the calculated Au–O_s + Au–Ti contributions (solid line) and calculated Au–O_l contribution (dashed line).

Table 1
EXAFS results characterizing TiO_2-supported mononuclear gold complexes[a]

Shell	N	R (Å)	$10^3 \times \Delta\sigma^2$ (Å)^2	ΔE_0 (eV)
Au–Au	–[b]	–	–	–
Au–O_s	2.0	2.16	6.05	−1.36
Au–O_l	0.8	3.26	9.30	−5.13
Au–Ti	0.5	2.77	3.54	10.16

[a]Notation: N, coordination number; R, distance between absorber and backscatterer atoms; $\Delta\sigma^2$, Debye–Waller factor; ΔE_0, inner potential correction.
[b]Undetectable.
Expected errors N: ± 10%, R: ± 0.02 Å, $\Delta\sigma^2$: ± 20%, ΔE_0: ± 20%. The subscripts s and l refer to short and long, respectively.

5. Discussion

5.1. Reduction of gold in supported catalysts during He and H_2 treatment

The XANES results showing a decrease in the area under the white line with increasing temperature of treatment in He or H_2 (figure 1) indicate increasing reduction of the cationic gold, ultimately forming metallic gold. The samples treated in He at 323 or 373 K show the presence of cationic gold with metallic gold, whereas the samples treated in flowing He at 473 or 573 K demonstrate the presence of metallic gold clusters without any indication of cationic gold. Consistent with these observations, autoreduction of supported metals (e.g., Pd clusters supported on zeolite Y [35] and copper-exchanged zeolite ZSM-5 [36]) has been shown to occur in He or vacuum, and it has been suggested to involve a charge-transfer transition from the support to the metal and the participation of hydroxyl groups of the support [27,28].

Similarly, the samples treated in flowing H_2 at 373, 473, or 573 K show the presence of metallic gold with no indication of cationic gold. Our results agree with previous reports showing the reduction of supported gold to the metallic state as a result of H_2 treatment [37,38]. The comparison of the samples treated in He with those treated in H_2 demonstrates a faster reduction of the cationic gold in H_2 than in He; the features characteristic of metallic gold in the XANES spectrum of the TiO_2-supported samples treated in H_2 appeared at temperatures as low as 373 K, whereas these features first appeared at about 473 K when the treatment gas was He.

In summary, the results demonstrate the presence of metallic gold after He or H_2 treatment at temperatures as low as 473 K of the sample initially containing cationic gold. Although the spectra do not give evidence of cationic gold remaining in the samples after the treatments, we emphasize that the XANES results are only qualitative, and we cannot rule out the possibility that some cationic gold remained.

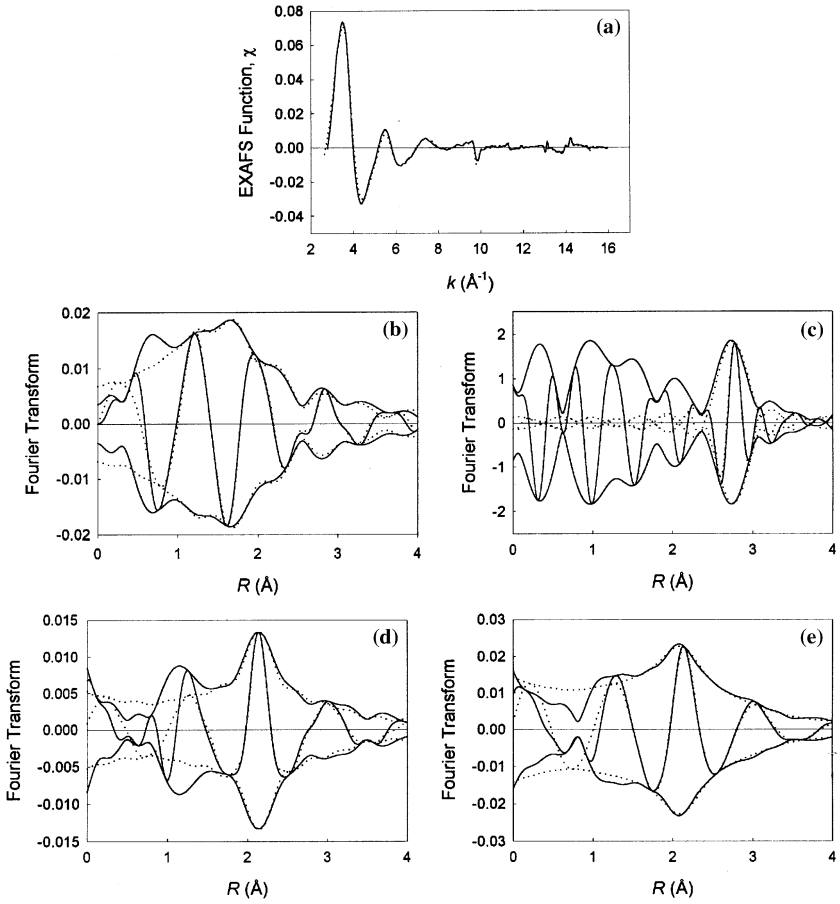

Figure 3. Results of EXAFS analysis characterizing the TiO_2-supported gold sample formed by adsorption of $Au(CH_3)_2(acac)$ at 1 atm and 298 K and subsequent treatment in flowing He at 373 K for 2 h: (a) Experimental EXAFS function (solid line) and sum of the calculated Au–Au + Au–Au(2nd) + Au–O_s + Au–O_1 contributions (dashed line). (b) Imaginary part and magnitude of uncorrected Fourier transform (k^0 weighted) of experimental EXAFS function (solid line) and sum of the calculated Au–Au + Au—Au(2nd) + Au–O_s +Au—O_1 contributions (dashed line). (c) Residual spectrum illustrating the Au–Au contribution; imaginary part and magnitude of phase- and amplitude-corrected Fourier transform (k^0 weighted) of experimental data minus the calculated Au–Au(2nd) + Au–O_s + Au–O_1 contributions (solid line) and calculated Au–Au contribution (dashed line). (d) Residual spectrum illustrating the Au–O_s contribution; imaginary part and magnitude of phase- and amplitude-corrected Fourier transform (k^0 weighted) of experimental data minus the calculated Au–Au + Au–Au(2nd) + Au–O_1 contributions (solid line) and calculated Au–O_s contribution (dashed line). (e) Residual spectrum illustrating the Au–O_1 contribution; imaginary part and magnitude of phase and amplitude-corrected Fourier transform (k^0 weighted) of experimental data minus the calculated Au–Au + Au–Au(2nd) + Au–O_s contributions (solid line) and calculated Au–O_1 contribution (dashed line).

5.2. *Cluster formation during He or H_2 treatment*

The EXAFS results demonstrate the aggregation of supported mononuclear gold complexes into supported gold clusters on the TiO_2 surface upon treatment in He or H_2; at the highest treatment temperature, clusters with an average diameter of about 15 Å formed, as demonstrated by the Au–Au first- and second-shell coordination numbers (table 2). Consistent with our results, gold on MgO and on γ-Al_2O_3 undergoes aggregation during treatment in He or H_2 at temperatures similar to those reported here, with the resultant clusters being somewhat larger than those formed on TiO_2 [39,40]. It has been suggested that the density of hydroxyl groups on an oxide support influences the aggregation of supported metal clusters, possibly by affecting the strength of the metal–support interaction and the rate of migration of the metal [41]. Thus, we suggest that the hydroxyl groups on the TiO_2 support, which was calcined at 673 K and initially had a significant fraction of its surface covered by OH groups [42], facilitate the aggregation of the gold.

5.3. *Stability of supported gold complexes and clusters during CO oxidation catalysis*

The XANES and EXAFS results demonstrate that the mononuclear Au(III) species were not stable during CO oxidation catalysis under our reaction conditions, as indicated by their reduction and aggregation during catalysis to form metallic gold clusters. In contrast, the sample that had been pretreated in He at 573 K to form metallic gold clusters of about the same average diameter (15 Å) did not undergo aggregation during

Table 2
EXAFS results characterizing the supported species formed by removal of ligands from $Au^{III}(CH_3)_2$(acac) and aggregation of the gold on TiO_2 after treament for 2 h in He or in H_2 at various temperatures[a]

Shell	Treament gas and conditions								
	He				Treatment temperature	H_2			
	N	R (Å)	$10^3 \times \Delta\sigma^2$ (Å^2)	ΔE_0 (eV)	(K)	N	R (Å)	$10^3 \times \Delta\sigma^2$ (Å^2)	ΔE_0 (eV)
					373				
Au–Au	5.1	2.84	10.35	0.10		5.2	2.82	8.39	0.92
Au–Au 2nd	1.0	4.04	1.92	0.15		1.0	4.02	0.61	1.29
Au–O_s	0.8	2.14	4.94	−2.00		0.9	2.14	1.51	−1.09
Au–O_1	1.1	2.75	1.49	8.05		0.8	2.72	7.62	4.26
					473				
Au–Au	6.3	2.83	8.03	0.11		6.8	2.82	7.21	1.62
Au–Au 2nd	2.0	4.05	10.13	6.63		1.9	4.04	6.71	2.03
Au–O_s	1.0	2.10	7.59	−1.95		1.0	2.08	8.13	2.89
Au–O_1	1.2	2.74	5.52	3.05	573	1.2	2.75	4.46	3.56
Au–Au	7.1	2.82	9.78	3.63		7.1	2.82	8.14	2.14
Au–Au 2nd	2.2	4.05	1.92	0.89		2.5	4.05	7.58	1.03
Au–O_s	0.1	1.95	10.12	2.47		0.1	1.95	11.89	2.16
Au–O_1	0.8	2.72	1.92	1.29		1.1	2.72	2.08	−1.95

[a]Notation as in table 1.

catalysis, as shown by EXAFS spectroscopy of the working catalyst. The data show retention of the initial cluster size, as indicated by the lack of changes in the first- and second-shell Au–Au coordination numbers.

The data are not sufficient to explain why the metallic gold clusters were resistant to further aggregation during catalysis, but strong interactions of small metal clusters with a support can stabilize them (as well as influencing their catalytic properties). Recent theoretical work shows that the Rh atoms in Rh_6 clusters at the interface with a zeolite support bear significant positive charges, whereas the Rh atoms not at the interface are nearly uncharged [43]. The metal cations at the interface bond the clusters to the supports. (The bonding of metal clusters to supports by cations can apparently be accentuated when the clusters contain oxophilic metals; thus, highly dispersed Pt–W clusters on γ-Al_2O_3 are stable at quite high temperatures as the oxophilic tungsten helps to maintain the high dispersion of the platinum [44].

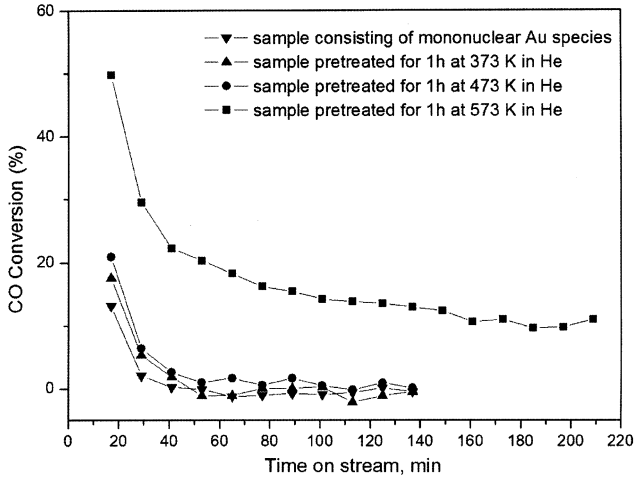

Figure 4. Oxidation of CO at 298 K in the presence of unpretreated as well as of the pretreated TiO_2-supported gold catalysts. Feed CO and O_2 partial pressures were 11 and 11 Torr, respectively; total feed flow rate was l00 mL min^{-1} (NTP); the mass of catalyst was 0.05 g.

It has been suggested that active species for CO oxidation in supported gold catalysts consist of structures that incorporate both Au^0 and Au^{n+}, possibly in Au^0–Au^{n+} clusters [45,46], and, because the XANES of gold supported on MgO indicated the presence of mixtures of cationic and zero-valent gold in the working catalysts [28], we do not rule out this possibility.

We postulate the occurrence of similar structures in our catalysts during reaction, consistent with an earlier speculation [46]. In such a structure, the arrangement of cationic and zero-valent gold in the supported structures would be expected to influence the chemisorption and catalytic properties of the material. We emphasize, however, that our data give no direct evidence for the cationic gold postulated to exist in these catalysts.

5.4. *Cluster size and oxidation states of gold in CO oxidation catalysts*

The catalytic performance of the as-prepared sample, initially containing mononuclear Au(III) complexes with no evidence of metallic gold clusters, was nearly the same as that of the sample that had been pretreated in He at 373 or 473 K (containing metallic gold clusters). Thus, the initial presence or absence of gold clusters (or gold complexes) had at most a minor effect on the catalytic performance. When the temperature of

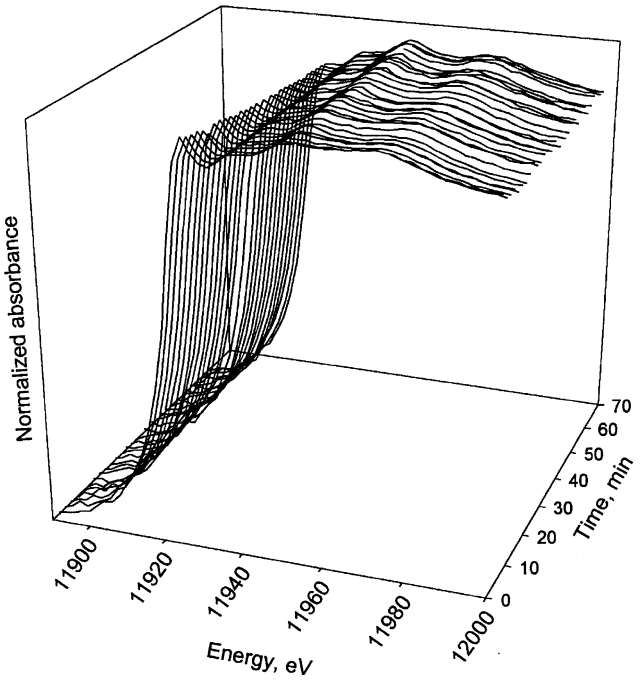

Figure 5. XANES data characterizing the initially prepared sample, containing TiO_2-supported Au(III) complexes, during CO oxidation catalysis at atmospheric pressure and at 373 K. Conditions of CO oxidation catalysis: 373 K, 760 Torr (11 Torr of O_2, 11 Torr of CO, and the balance He), and the total feed flow rate was 100 mL (NTP) min^{-1}.

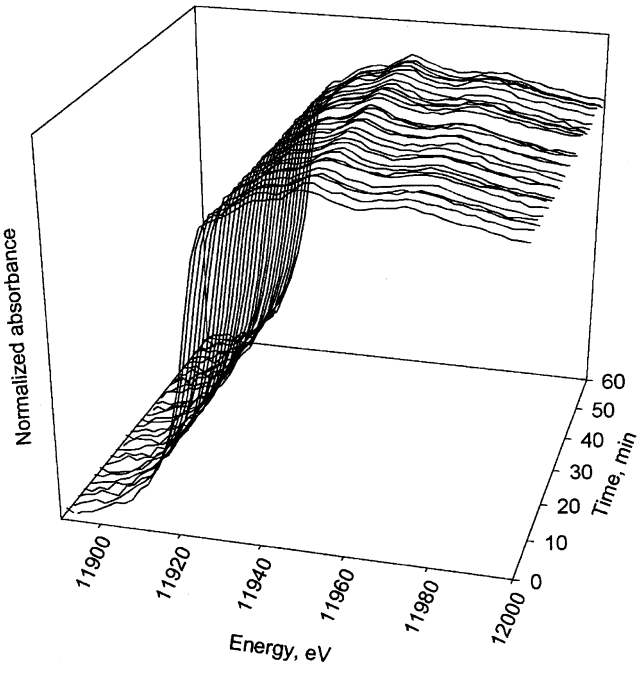

Figure 6. XANES data characterizing the samples that had been treated in He at 573 K, containing gold clusters, during CO oxidation catalysis at atmospheric pressure and at 373 K. Conditions of CO oxidation catalysis: 373 K, 760 Torr (11 Torr of O_2, 11 Torr of CO, and the balance He); the total feed flow rate was 100 mL (NTP) min^{-1}.

treatment in He was increased to 573 K, giving a sample containing gold clusters with an average diameter of about 15 Å (as estimated from the Au–Au first-shell contribution of about 7), the catalytic activity was markedly higher (figure 4), and, in contrast to the catalysts mentioned in the preceding sentence, the catalyst did not deactivate completely in the flow reactor experiments.

These results suggest an influence of the gold cluster size on the catalytic activity – but only for clusters larger than about 12 Å in average diameter. The clusters in the sample containing the larger clusters (about 15 Å in average diameter) were found to be stable during CO oxidation catalysis, and the XANES data give no evidence of cationic gold in this sample. Nor was there XANES evidence of the catalysts characterized by the smaller average cluster size, and this sample deactivated completely during the first hour of operation. Thus, one sample containing metallic gold was a stable catalyst and another was not. Furthermore, during catalysis with the as-prepared sample, metallic gold clusters formed, but the data suggest that the size of these clusters (with an Au–Au first-shell coordination number less than about 7, corresponding to an average diameter less than about 15 Å) did not significantly affect the catalytic activity for CO oxidation. The lack of a simple pattern of changing activity with changing average cluster size suggests that metallic gold alone is not the catalytically active species for CO oxidation and raises the question of whether there is a significant variable in addition to gold cluster size, such as the gold oxidation state(s).

One might expect a correlation: the higher the temperature of treatment, the higher would be the degree of reduction and aggregation of the gold. The catalytic activity could depend on the surface area of the metallic gold and perhaps also on the amount of cationic gold associated with the zerovalent gold [28,46]. But if there were greater reduction of the gold at the higher treatment temperature, one might expect a lower catalytic activity, corresponding to the smaller amount of cationic gold and perhaps the lower surface area of zerovalent gold. The data do not correspond to this expectation, perhaps because the larger metallic gold particles are relatively inactive [9,47], although there may be an optimum cluster size [19,37]. One might reason that the higher-temperature treatments cause greater dehydroxylation of the support, and if support OH groups play a role in the catalysis, as has been suggested [48], then there would be fewer of them expected after the higher-temperature treatment. The observations do not support this suggestion because the sample treated at the higher temperature had the highest activity, but, again, there could be complicating effects of cluster size.

Another possibility is that there was some reoxidation of the gold by support OH groups (perhaps increasingly at higher treatment temperatures), leading to fragmentation of the gold and formation of cationic gold

Table 3
EXAFS results characterizing the TiO_2-supported gold species before and during CO oxidation catalysis at atmospheric pressure and at 373 K[a]

Backscatter	TiO_2-supported gold species							
	Before CO oxidation catalysis				During CO oxidation catalysis[b]			
	N	R (Å)	$10^3 \times \Delta\sigma^2$ (Å^2)	ΔE_0 (eV)	N	R (Å)	$10^3 \times \Delta\sigma^2$ (Å^2)	ΔE_0 (eV)
Au								
1st shell	–[c]	–	–	–	7.0	2.82	2.32	2.56
2nd shell	–	–	–	–	2.0	4.05	4.25	4.58
Support								
O_s	2.0	2.16	6.05	−1.36	0.2	1.95	3.62	4.61
O_l	0.8	3.26	9.30	−5.13	1.0	2.72	4.26	5.72
Ti	0.5	2.77	3.54	10.16	–[c]	–	–	–

[a]Notation as in table 1.
[b]During steady-state operation, after 1 h TOS. Conditions of CO oxidation catalysis: 373 K, 760 Torr (11 Torr of O_2, 11 Torr of He, and the balance He); the total feed flow rate was 100 mL (NTP) min^{-1}.
[c]Undetectable.

Table 4
EXAFS characterization the TiO_2-supported gold species formed by treatment in He at 573 K before and during CO oxidation catalysis at atmospheric pressure and 373 K[a]

Backscatterer	TiO_2-supported gold species formed by treatment in He at 573 K							
	Before CO oxidation catalysis				During CO oxidation catalysis[b]			
	N	R (Å)	$10^3 \times \Delta\sigma^2$ (Å^2)	ΔE_0 (eV)	N	R (Å)	$10^3 \times \Delta\sigma^2$ (Å^2)	ΔE_0 (eV)
Au								
1st shell	7.1	2.82	9.78	3.63	7.3	2.82	5.13	2.52
2nd shell	2.2	4.05	1.92	0.89	2.5	4.04	2.43	2.12
Support								
O_s	0.1	1.95	10.12	2.47	0.2	1.96	6.32	3.56
O_l	0.8	2.72	1.92	1.29	0.7	2.71	5.24	3.53

[a]Notation as in table 1.
[b]During steady-state operation, after 1 h TOS. Conditions of CO oxidation catalysis: 373 K, 760 Torr (11 Torr of CO and of O_2, and the balance He; the total feed flow rate was 100 mL (NTP) min^{-1}.

(similar chemistry of supported rhodium is well known [14]); this suggestion would perhaps account for the higher activity of the samples treated at the higher temperatures, corresponding to more cationic gold in these samples. We emphasize that this suggestion implies both autoreduction of the gold and oxidation of the gold on the support. This suggestion is consistent with catalysis at the interface between the (hydroxylated) support and the gold clusters [46,48].

In summary, the catalytic properties of TiO_2-supported gold are evidently not simply related to the gold cluster size, and there is less than sufficient evidence to determine any role of cationic gold in CO oxidation catalysis by these samples.

6. Conclusions

We report a synthesis method that allows control of the average size of TiO_2-supported gold nanoclusters made from adsorbed $Au^{III}(CH_3)_2$(acac) and their characterization by XANES and EXAFS spectroscopies. XANES and EXAFS data demonstrate the formation of mononuclear Au(III) complexes as the predominant surface gold species upon adsorption of $Au^{III}(CH_3)_2$ (acac) on TiO_2. The mononuclear complex is bonded to two oxygen atoms, which are inferred to be part of the TiO_2 surface, with an Au–O distance of 2.16 Å. Treatment of the initially prepared TiO_2-supported gold species in He and H_2 at increasing temperatures and 1 atm led to formation of metallic gold clusters of increasing size, ultimately those with an average diameter of about 15 Å. The data demonstrate the presence of metallic gold clusters in the working catalysts, but they also show the clusters alone are not responsible for the catalytic activity.

Acknowledgments

S. Kuba thanks the Alexander von Humboldt Foundation for a Feodor Lynen fellowship. This research was

supported by the U.S. Department of Energy, Office of Energy Research, Office of Basic Energy Sciences, Division of Chemical Sciences, Contract FG02-87ER13790. We acknowledge the National Synchrotron Light Source, Brookhaven National Laboratory, which is supported by the U.S. Department of Energy, Division of Materials Sciences and Division of Chemical Sciences, under Contract No. DE-AC02-98CH10886, and the staff of beamline X-11A. The EXAFS data were analyzed with the XDAP software [18].

References

[1] M. Haruta, S. Tsubota, T. Kobayashi, H. Kageyama, M.J. Genet and B. Delmon, J. Catal. 144(1993)175.
[2] S.D. Lin, M.A. Bollinger and M.A. Vannice, Catal. Lett. 17 (1993) 245.
[3] H. Liu, A.I. Kozlov, A.P. Kozlova, T. Shido and Y. Iwasawa, Phys. Chem. Chem. Phys. 1 (1999) 2851.
[4] E.E. Stangland, K.B. Stavens, R.P. Andres and W.N. Delgass, J. Catal. 191 (2000) 332.
[5] G. Mul, A. Zwijnenburg, B. van der Linden, M. Makkee and J.A. Moulijn, J. Catal.201 (2001) 128.
[6] N.W. Cant and N.J. Ossipoff, Catal. Today 36 (1997) 125.
[7] B. Nkosi, N.J. Coville and G.J. Hutchings, J. Chem. Soc., Chem. Commun. 1 (1988) 71.
[8] M.M. Schubert, S. Hackenberg, A.C, van Veen, M. Muhler, V. Plzak and R.J. Behm, J. Catal. 197 (2001) 113.
[9] M. Haruta, Catal. Today 36 (1997) 153.
[10] A.P. Kozlova, A.I. Kozlov, S. Sugiyama, Y. Matsui, K. Asakura and Y. Iwasawa, J. Catal. 181 (1999) 37.
[11] M. Maciejewski, P. Fabrizioli, J.-D. Grunwaldt, O.S. Becker and A. Baiker, Phys. Chem. Chem. Phys. 3 (2001) 3846.
[12] B. Schumacher, V. Plzak, M. Kinne and R.J. Behm, Catal. Lett. 89 (2003) 109.
[13] This compound was first used to prepare supported gold by M. Okumura, K. Tanaka, A. Ueda and M. Haruta, Solid State Ionics 95 (1997) 143. Pyrolysis of $Au(CH_3)_2(acac)$ was observed to occur, and the gold aggregated to form nanoparticles.
[14] F.S. Lai and B.C. Gates, Nano Lett. 1 (2001) 583.
[15] W. A. Weber and B. C. Gates, J. Phys. Chem. B 101 (1997) 10423.
[16] J.B.A.D, van Zon, D.C. Koningsberger, H.F.J. van't Blik and D.E. Sayers, J. Chem. Phys. 82(1985)5742.
[17] P.S. Kirlin, F.B.M. van Zon, D.C. Koningsberger and B.C. Gates, J. Phys. Chem. 94 (1990) 8439.
[18] M. Vaarkamp, J.C. Linders and D.C. Koningsberger, Physica B 209 (1995) 159.
[19] D.E. Ramaker, B.L. Mojet, D.C. Koningsberger and W.E. O'Grady, J. Phys. Condens. Matter 10 (1988) 8753.
[20] D.E. Ramaker, X. Quan and W.E. O'Grady, Chem. Phys. Lett. 299 (1999) 221.
[21] J.W. Cook Jr. and D.E. Sayers, J. Appl. Phys. 52 (1981) 5024.
[22] F.B.M. Duivenvoorden, D.C. Koningsberger, Y.S. Uh and B.C. Gates, J. Am. Chem. Soc. 108 (1986) 6254.
[23] (a) S.I. Zabinsky, J.J. Rehr, A. Ankudinov, R.C. Albers and M.J. Eller, Phys. Rev. B 52 (1995) 2995. (b) A. Ankudinov, Ph. D. Dissertation, University of Washington, 1996.
[24] J.D.H. Donnay and H.M. Ondik, *Crystal Data Determinative Tables*, 3rd ed., Vol. II U.S. Dept. of Commerce, National Bureau of Standards and the Joint Committee on Powder Diffraction Standards: U.S.A., 1973) p. C-88.
[25] F.B.M. van Zon, S.D. Maloney, B.C. Gates and D.C. Koningsberger, J. Am. Chem. Soc. 115 (1993) 10317.
[26] J. B. A. D. van Zon, Ph.D. Dissertation, Eindhoven University of Technology, The Netherlands, 1988.
[27] F.W. Lytle, D.E. Sayers and F, A. Stern, Physica B 158 (1989) 701.
[28] J. Guzman and B.C. Gates, J. Phys. Chem. B 106 (2002) 7659.
[29] R.E. Benfiled, D. Grandjean, M. Kröll, R. Pugin, T. Sawitowski and G. Schmid, J.Phys. Chem. B 105 (2001) 1961,
[30] T.M. Salama, T. Shido, R. Ohnishi and M. Ichikawa, J. Phys. Chem. 100 (1996) 3688.
[31] J. Guzman and B.C. Gates, Angew. Chem. Int. Ed. 42 (2003) 690.
[32] J.F. Goellner, B.C. Gates, G.N. Vayssilov and N. Rösch, J. Am. Chem. Soc. 122 (2000) 8056.
[33] P. Serp, P. Kalck and R. Feurer, Chem. Rev. 102 (2002) 3085.
[34] (a) B.J. Kip, F.B.M. Duivenvoorden, D.C. Koningsberger and R. Prins, J. Catal. 105 (1987) 26; (b) A. Jentys, Phys. Chem. Chem. Phys. 1 (1999) 4059.
[35] W. Vogel, H. Knözinger, B.T. Carvill, W.M.H. Sachtler and Z.C. Zhang, J. Phys. Chem. B 102(1998) 1750.
[36] S. Hu, J.A. Reimer and A.T. Bell, J. Phys. Chem. B 101 (1997) 1869.
[37] G.C. Bond and D.T. Thompson, Catal. Rev-Sci. Eng. 41 (1999) 319.
[38] S. Galvagno and G. Parravano, J. Catal. 55 (1978) 178.
[39] J. Guzman and B.C. Gates, Nano Lett. 1 (2001) 689.
[40] J. Guzman and B.C. Gates, Langmuir 19 (2003) 3897.
[41] B.C. Gates, J. Mol. Catal. A 163 (2000) 55.
[42] J.F. Goellner, J. Guzman and B.C. Gates, J. Phys. Chem. B 106 (2002) 1229.
[43] G.N. Vayssilov, B.C. Gates and N. Rösch, Angew. Chem. Int. Ed. 42 (2003) 1391.
[44] O. Alexeev, G.W. Graham, M. Shelef and B.C. Gates, J. Catal. 190 (2000) 157.
[45] C.K. Costello, M.C. Kung, H.-S. Oh, Y. Wang and H.H. Kung, Appl. Catal. A 232 (2002) 159.
[46] G.C. Bond and D.T. Thompson, Gold Bull. 33 (2000) 41.
[47] M. Valden, X. Lai and D.W. Goodman, Science 281 (1998) 1647.
[48] C.K. Costello, J.H. Yang, H.Y. Law, Y. Wang, J.-N. Lin, L.D. Marks, M.C. Kung and H.H. Kung, Appl. Catal. A 243 (2003) 15.